Industrial Chemistry & Materials

ROYAL SOCIETY OF CHEMISTRY

PAPER

View Article Online
View Journal | View Issue

Cite this: *Ind. Chem. Mater.*, 2025, **3**, 57

Toward a low-cost uranium-adsorbing material based on nonwoven fabrics and photografting technology†

Zhiwei Zhong, Yanbin Huang * and Wantai Yang*

Amidoxime-functionalized polymeric adsorbents have attracted great interest for uranium extraction from seawater. However, the current graft polymerization method is time-consuming (2–6 h), wasteful in reagent, and hence not economical. Here, amidoxime-functionalized adsorbents based on low-cost polypropylene melt-blown nonwoven fabric (MBF) are produced by a simple, fast and also low-cost surface photografting technology, by which more than 80% of reagents can be saved and grafting time can be reduced to 3 min. The fabricated adsorbents retain their mechanical properties and exhibit excellent uranium adsorption properties, with a maximum uranium adsorption capacity of 400 mg g^{-1} when the monomer ratio of AN to AA is 8 : 2. Moreover, we showed that the adsorbents could be either reused or simply incinerated for uranium recovery. The photografting technology has great potential for low-cost, continuous industrial production of uranium-adsorbing material.

Received 29th March 2024,
Accepted 26th July 2024

DOI: 10.1039/d4im00034j

rsc.li/icm

Keywords: Uranium extraction from seawater; Amidoxime; Nonwoven fabric; Surface photografting.

1 Introduction

Nuclear power plays a crucial role in supplying clean energy, characterized by its capacity to consistently generate substantial electricity with minimal CO_2 emissions.[1] However, the terrestrial uranium resource, which is the essential material for nuclear power generation, is finite and projected to be depleted in about a century.[2] Fortunately, seawater contains approximately 4.5 billion tons of uranium, roughly 1000 times more than that found on land, making uranium extraction from seawater an appealing alternative.[3] Over the past decades, many approaches have been explored for extracting uranium from seawater, including adsorption,[3–12] membrane separation,[13] ion exchange,[14] electrochemical deposition,[15,16] *etc.* Among these, the adsorption method stands out as the most promising for industrial applications, given its cost-effectiveness, high efficiency, and straightforward operational procedures.

The key aspect of the adsorption method lies in the utilization of uranium adsorbent materials with high selectivity and adsorption capacity. Research on uranium extraction from seawater started in the 1950s, with early efforts using inorganic adsorbents such as hydrous titanium dioxide.[17] In 1979, Egawa *et al.* reported the first amidoxime-functionalized polymeric adsorbent.[18] Subsequent studies demonstrated that the amidoxime moiety exhibits outstandingly strong affinity and high selectivity for uranium.[19,20] Since then, amidoxime-functionalized polymeric adsorbents have gained widespread acceptance as the most promising materials for large-scale uranium extraction from seawater.[21]

Various methods for preparing amidoxime-functionalized polymeric adsorbents have been developed, and they can be broadly categorized into two types. One approach is to first synthesize amidoxime-containing polymers and then make the polymers into devices like microspheres,[22] fibers,[23–26] membranes,[27,28] *etc.* Adsorbents prepared in this manner exhibit a high density of amidoxime groups and impressive adsorption capacity, but often suffer from poor mechanical properties and alkali resistance due to the nature of the materials. The other approach is to use pre-made, inexpensive polyolefin fibers or membranes with robust mechanical properties as a substrate, and introduce amidoxime groups only on their surface.[29–31] Currently, radiation-induced graft polymerization (RIGP) is the most widely used method for grafting amidoxime groups onto substrates. The RIGP process encompasses three steps: (1) generating free radicals on the substrate's surface through electron beams or high-energy ray irradiation; (2) immersing the substrate with surface free radicals in an acrylonitrile and co-monomer solution for surface graft polymerization; and (3) converting the cyano group to the amidoxime group

Department of Chemical Engineering, Tsinghua University, Beijing 100084, China. E-mail: yanbin@tsinghua.edu.cn, yangwantai@tsinghua.edu.cn

† Electronic supplementary information (ESI) available. See DOI: https://doi.org/10.1039/d4im00034j

through reaction with hydroxylamine. However, the RIGP method has two significant limitations. Firstly, high-energy rays require specialized equipment and can lead to substantial degradation of the material's mechanical properties.[32] Secondly, the surface graft polymerization in solution is reagent wasteful (only micron-thick monomers are needed for surface grafting, the rest are mostly wasted or homopolymerized) and time-consuming, typically requiring 2–6 h for the degree of grafting to exceed 100%.[33,34]

Compared with the radiation-induced surface grafting approach, surface photografting polymerization is much simpler, milder, and easier to operate. However, to the best of our knowledge, there are few studies utilizing surface photografting polymerization for the preparation of amidoxime adsorbents. Na *et al.* reported the preparation of amidoxime adsorbents by immersing polypropylene fabrics in an acrylonitrile and benzophenone solution, initiating polymerization through irradiation with a high-pressure mercury lamp.[35] However, surface photografting reactions in solution also show low monomer utilization and photografting rate, reaching a maximum grafting rate of less than 80% even after 5 h of irradiation. Rather than immersing the substrate in bulk solution, there is actually an alternative photografting process, bulk surface photografting polymerization (BSPP),[36,37] where the reaction solution is applied to the polymer surface in ultra-thin layers (in the order of micrometers) through a sandwich structure setup. This process offers several advantages: (1) it has high grafting efficiency and fast reaction by maximizing the contact between the surface and the photo-excited reagents; (2) the required amount of reaction solution is very low, resulting in higher reagent utilization.

In this study, we fabricated amidoxime adsorbents from low-cost polypropylene melt-blown nonwoven fabric (MBF) by a simple, fast and also low-cost bulk surface photografting method, and evaluated their performance in uranium adsorption. MBF is selected as the substrate owing to its large specific surface area, low price, and outstanding mechanical properties. The process of bulk surface photografting polymerization facilitates the rapid introduction of abundant cyano groups onto the polymer fibers' surface using minimal reagents. After the transformation into amidoxime-functionalized adsorbents, we evaluated their adsorption kinetics, thermodynamics, and metal ion selectivity along with the influence of amidoxime groups and hydrophilic groups on the adsorption properties. The findings demonstrated that bulk surface photografting polymerization serves as a simple, swift and efficient method to prepare uranium adsorbent materials.

2 Results and discussion

In order to improve the diffusion of uranyl ions in the surface layer of the adsorbent and thus the uranium adsorption capacity,[38] a series of adsorbents containing different amounts of hydrophilic carboxyl groups along with amidoxime groups are prepared. The schematic diagram for the synthesis of amidoxime-functionalized MBF adsorbents is shown in Scheme 1. Firstly, acrylonitrile (AN) and acrylic acid (AA) mixed solution (5 μL mg^{-1} MBF, about 4 mg reagent per mg MBF) is added dropwise to the surface of the MBF, and the cyano and carboxyl groups are introduced into the fiber surface by bulk surface photografting polymerization. After photografting, the MBF-g-P(AN-*co*-AA) is washed repeatedly with DMF to remove the homopolymer until the sample weight no longer changes. Later, by reacting with hydroxylamine, the cyano groups are converted into amidoxime groups.

2.1 Preparation of MBF-g-P(AN-*co*-AA) *via* bulk surface photografting

The ATR-FTIR spectra of the MBF before and after bulk surface photografting are shown in Fig. 1a. In all samples, the characteristic peaks of the $-CH_3$ (2957 cm^{-1}, 2871 cm^{-1}, 1378 cm^{-1}) and $-CH_2-$ (2916 cm^{-1}, 2843 cm^{-1}, 1460 cm^{-1}) of polypropylene are evident. After bulk surface photografting, a distinct peak at 2243 cm^{-1} corresponding to C≡N suggests the successful grafting of AN onto the MBF. Furthermore, after the photografting reaction with AA included in the reaction solution, the appearance of characteristic peaks of C=O (1726 cm^{-1}) and C–O (1166–1241 cm^{-1}) confirms the successful grafting of AA onto the MBF. In order to further elucidate the chemical structure of the MBF after photografting, the ratios of C=O to C≡N absorption peak intensity are calculated for different monomer ratios. As the AA concentration increases, the proportion of AA chain segments in the grafted polymer chain also increases, as evidenced by the rise in the Abs(C=O)/Abs(C≡N) ratio in Fig. 1b.

The successful photografting of AA and AN is further substantiated by XPS results. Fig. 1c compares the XPS survey spectra of the MBF before and after photografting. The untreated MBF exhibits only a characteristic XPS signal for carbon, while after bulk surface photografting, new characteristic peaks for nitrogen (N) and oxygen (O) are evident in the spectra. Fig. 1d presents the result of the

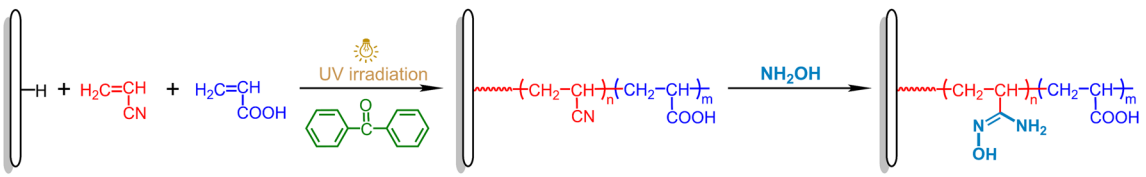

Scheme 1 Schematic diagram for the synthesis of amidoxime MBF adsorbents.

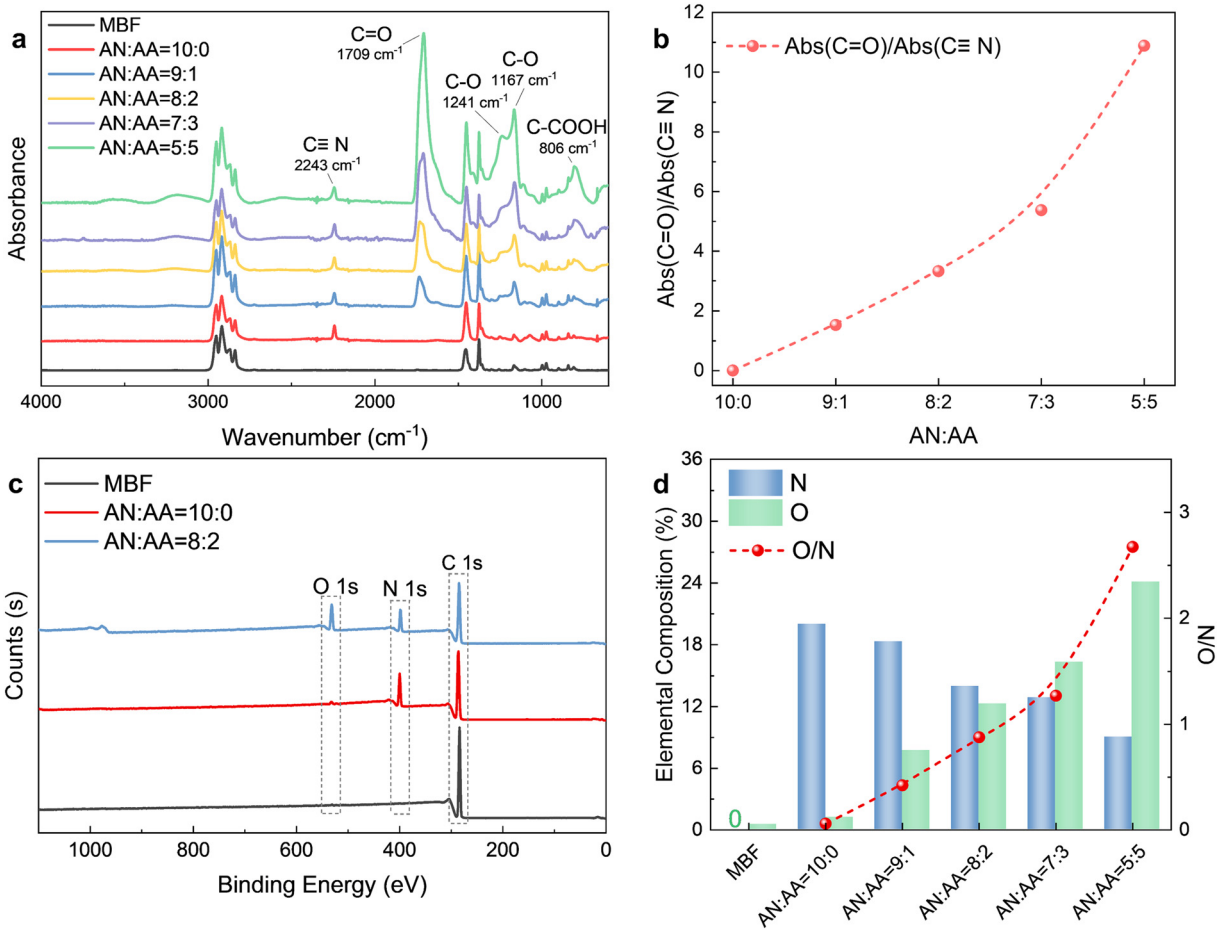

Fig. 1 (a) The FTIR spectra of the MBF before and after bulk surface photografting with different AN and AA monomer ratios; (b) the ratio of C═O to C≡N absorption peak intensity for different monomer ratios; (c) XPS survey spectra and (d) elemental composition for the MBF before and after photografting.

semiquantitative XPS analysis, including elemental composition and O/N ratios. As the monomer ratio AN : AA varies from 10 : 0 to 5 : 5 (v/v), the N and O atomic percentages of the MBF-g-P(AN-*co*-AA) correspondingly decrease and increase, respectively. Consistent with the FTIR results, the O/N ratio gradually rises from zero. According to the XPS findings, it can be inferred that when the feeding monomer ratio is AN : AA = 8 : 2 (v/v), the molar ratio of C≡N to –COOH on the MBF-g-P(AN-*co*-AA) approaches 2 : 1, suggesting that AA has higher photografting polymerization reactivity than AN.

2.2 Factors affecting the photografting reaction

The influence of the irradiation time, the BP concentration, the monomer concentration and the composition on the

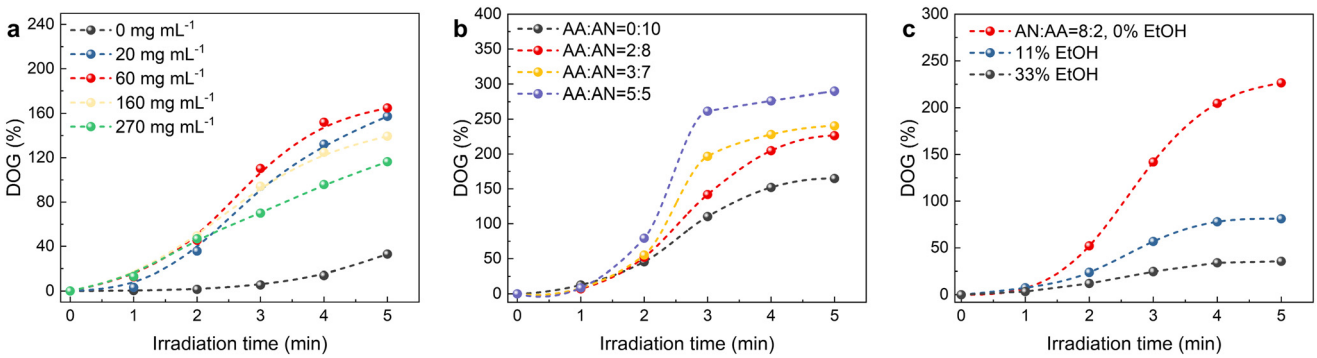

Fig. 2 Effect of the irradiation time, (a) BP concentration, (b) monomer composition and (c) concentration on the DOG.

grafting polymerization is presented in Fig. 2. In the absence of the photosensitizer BP, minimal photografting occurs, with a degree of grafting (DOG) of only 33% even after 5 min, as shown in Fig. 2a, while with the addition of 60 mg mL^{-1} BP, which abstracts the hydrogen atom from the surface polymer chain to form polymer radicals and initiate photografting, the DOG reaches 110% within 3 min. However, higher concentrations of BP hinder the photoreaction due to the self-shielding effect of BP.[39] Fig. 2b illustrates the effect of monomer composition (the volume ratio of AN and AA) on photografting. Given the higher reactivity of AA compared to AN, the photografting polymerization rate increases with AA content in the reaction solution. Monomer concentration is also a crucial factor affecting photografting, as shown in Fig. 2c. The fastest photografting reaction occurs at 100% monomer concentration (*i.e.*, under solvent-free conditions). Dilution of the monomer with ethanol results in a significant reduction in the reaction rate. Considering the time and cost of the process, subsequent photografting experiments are conducted with a BP concentration of 60 mg mL^{-1} and under solvent-free conditions. Notably, utilizing bulk surface photografting allows achieving a DOG exceeding 100% within 3 min, which may make continuous production feasible in the future, whereas other solution graft polymerization methods typically require several hours. In addition to saving time and allowing continuous production, our method (4 kg reagent per kg fabric) also saves about 80% of reagents compared to the grafting of fabrics immersed in solution (25 kg reagent per kg fabric).[40] Moreover, unlike RIGP, which employs high-energy radiation and results in a significant reduction of the substrate's mechanical properties, surface photografting is a milder process that avoids this degradation. In fact, the grafted polymer shell actually increases the tensile strength of the nonwoven fabric from 7.4 MPa to 15.8 MPa (Fig. S1†). Thus, bulk surface photografting is a faster, milder and cheaper approach compared to RIGP.

2.3 Fiber morphology

Fig. 3 shows the SEM images of MBF-g-P(AN-*co*-AA) fibers with different DOGs. The diameter of the MBF-g-P(AN-*co*-AA) fibers is obviously larger with the increase of the DOG. The DOG is related to the increase in the fiber volume before and after grafting and should be approximately proportional to the ratio of the square of the fiber diameter. For example, when the DOG is 168%, the fiber diameter increases to 2.9 μm (fiber diameter mode counted in the SEM image). The DOG calculated from this diameter is 133%, which is similar to the experimental value. The error may come from the density variation and fiber diameter distribution. The increase in fiber diameter reduces the specific surface area of the fabric from 1.4 $m^2\ g^{-1}$ to 0.9 $m^2\ g^{-1}$ after photografting. The SEM images and experimental data confirm that the grafting layer is formed primarily on the fiber surface (*i.e.*, with little material in the fabric voids), making the MBF-g-P(AN-*co*-AA) maintain the fiber morphology and the large specific surface area for uranium adsorption.

2.4 Preparation of MBF-g-P(AO-*co*-AA)

The preparation of MBF-g-P(AO-*co*-AA) *via* the amidoximation of MBF-g-P(AN-*co*-AA) is achieved through the nucleophilic addition of NH_2OH to the cyano groups. Fig. 4a shows the FTIR spectra of the MBF-g-P(AN-*co*-AA) after reaction with hydroxylamine at 60 °C for different durations. The C≡N peak at 2242 cm^{-1} significantly weakens after 1 h of reaction and

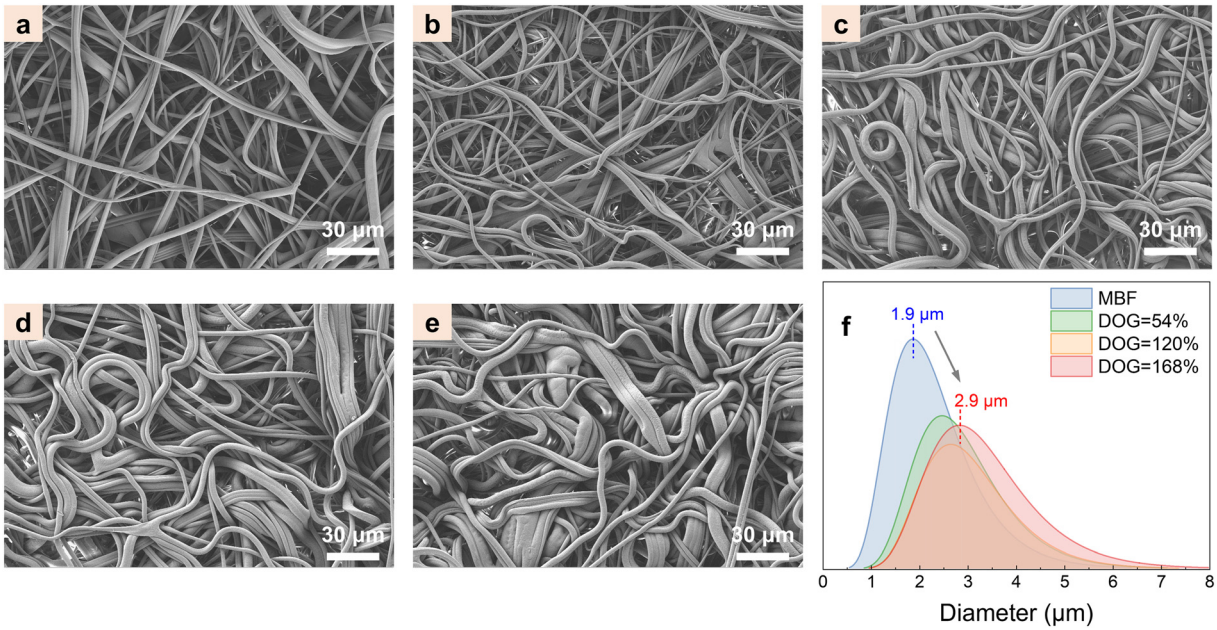

Fig. 3 SEM images of (a) MBF, DOG = 11% (b), 54% (c), 120% (d), and 168% (e); (f) diameter of MBF and MBF-g-P(AN-*co*-AA) with different DOGs.

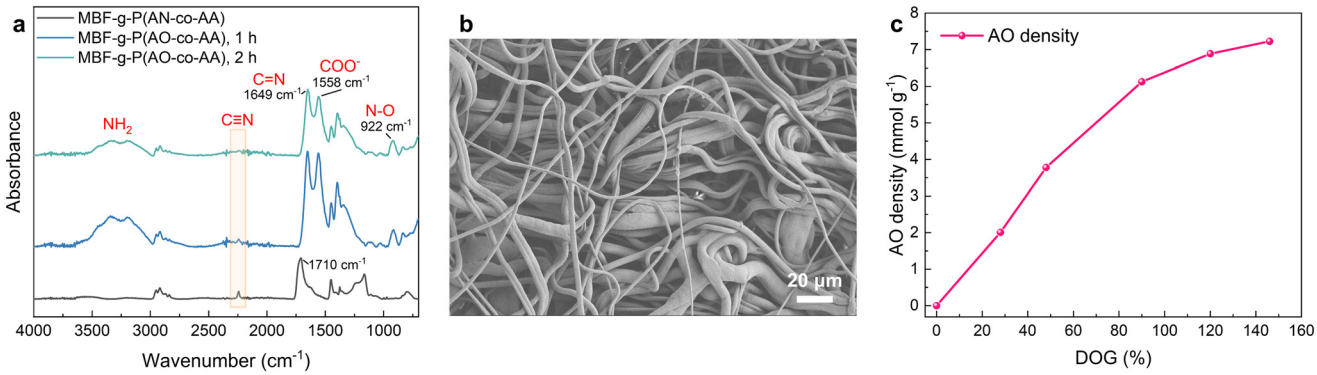

Fig. 4 (a) The FTIR spectra, (b) SEM image and (c) AO density of the fabric after reaction with hydroxylamine.

completely disappears after 2 h. Meanwhile, a strong characteristic peak of C═N and a characteristic peak of N–O appears at 1649 cm^{-1} and 922 cm^{-1}, respectively. The results indicate that the C≡N is completely converted to the amidoxime group (–$C(NH_2)$≡N–OH) within 2 h. Additionally, the characteristic peak at 1710 cm^{-1} disappears and a new peak appears at 1558 cm^{-1}, attributed to the conversion of the –COOH to –COONa caused by NaOH in the NH_2OH aqueous solution. The SEM image of MBF-g-P(AO-*co*-AA) (Fig. 4b) shows that the surface morphology has not significantly changed compared to MBF-g-P(AN-*co*-AA). As shown in Fig. 4c, the calculated AO density on fabrics gradually increases to 7 mmol g^{-1} as the DOGs increase to 140%. The amidoximation reaction reduces the tensile strength of the fabric to 11.9 MPa, which is still higher than the mechanical strength before grafting (Fig. S1†). It remains to be tested whether or not the material is strong and stable enough in actual seawater environment. Fortunately, our method is applicable to most polymer materials containing C–H bonds. Therefore, it is possible to select substrates with better mechanical properties to improve the stability and durability of the material.

2.5 Uranium adsorption performance

To assess the uranium adsorption capacity of the fabric, the MBF-g-P(AO-*co*-AA) is immersed in a 20-ppm uranium solution for adsorption experiments. In a typical example (Fig. 5a), the colour of the MBF-g-P(AO-*co*-AA) fabrics changes from white to yellow after the adsorption experiment. Furthermore, distinct characteristic peaks of uranium emerge in the XPS spectrum (Fig. 5b), indicating the successful adsorption of uranium onto MBF-g-P(AO-*co*-AA). Uranium adsorption capacity increases and

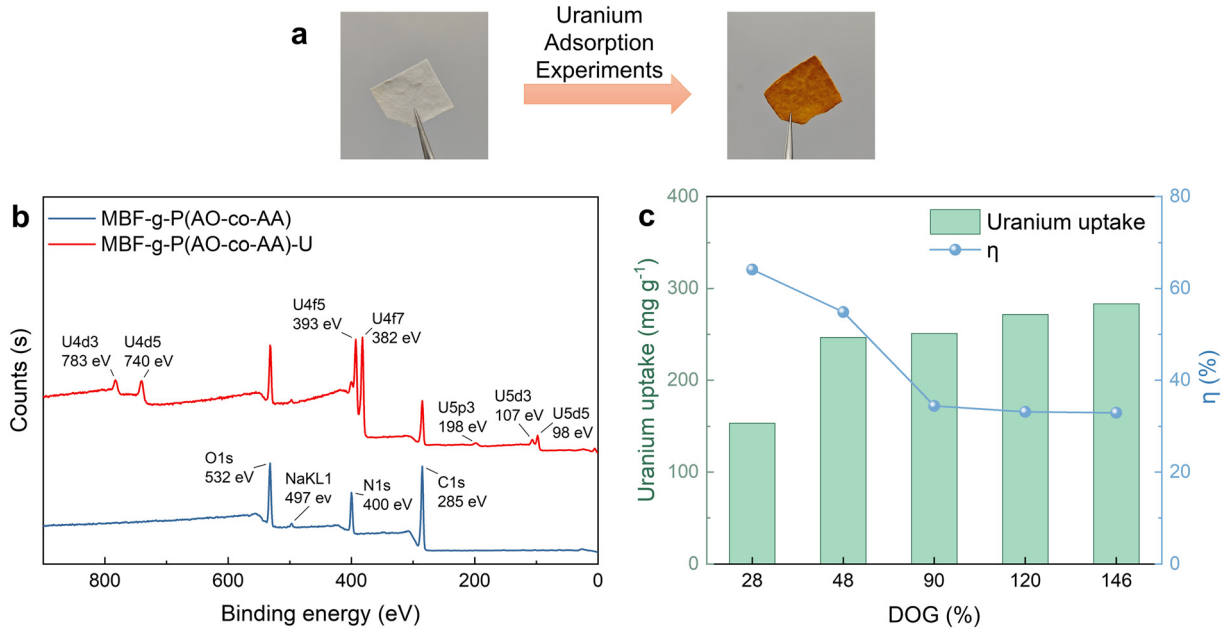

Fig. 5 (a) Images and (b) XPS spectra of MBF-g-P(AO-*co*-AA) before and after adsorption experiments; (c) adsorption capacity and amidoxime group utilization rate (η = 2q/238.03AO, where 2 represents the theoretical coordination where two amidoxime groups bind to one uranyl ion, 238.03 is the atomic mass of uranium (g mol^{-1}), and q and AO represent the actual uranium adsorption capacity (mg g^{-1}) and the amidoxime densities (mmol g^{-1}), respectively) of adsorbents with different DOGs.

then levels off with increasing DOG, while the utilization efficiency of the amidoxime groups decreases (Fig. 5c). This is due to the fact that the internal amidoxime groups are less accessible for uranium adsorption.

To investigate the effect of the chemical structure on the uranium adsorption properties, the MBF-g-P(AO-*co*-AA) prepared with different AN/AA monomer ratios (v/v) have been tested. As mentioned earlier, the feeding monomer ratio determines the C≡N-to-(–COOH) ratio in the graft layer, that is, the ratio of the amidoxime group to the carboxyl group. Fig. 6a shows that at AN : AA = 8 : 2, which means that the ratio of C≡N to –COOH is close to 2 : 1, the MBF-g-P(AN-*co*-AA) exhibits maximum uranium adsorption performance (251 mg g^{-1}). The carboxyl group, as a hydrophilic group and a hard Lewis base with the potential to coordinate with uranyl ions, helps to improve the uranium adsorption performance of the material. However, further increase of the –COOH groups leads to a decrease in the amount of amidoxime groups and is unfavourable for uranium adsorption. Therefore, unless otherwise specified, the following adsorption tests use the MBF-g-P(AO-*co*-AA) prepared with a monomer ratio of AN : AA = 8 : 2.

The uranium adsorption kinetics of both MBF-g-P(AO-*co*-AA) and MBF-g-PAO are shown in Fig. 6b. The amount of uranium adsorption gradually increases over time until reaching adsorption equilibrium at approximately 24 h. To explore the adsorption mechanism, the data are fitted to pseudo-first-order and pseudo-second-order kinetic models. As presented in Table 1, the correlation coefficient of the pseudo-second-order model (R^2 = 0.992) is higher than that of the pseudo-first-order model (R^2 = 0.9796), suggesting that the adsorption process is more consistent with the pseudo-second-order adsorption kinetic model. Moreover, the fitted equilibrium adsorption capacity of the pseudo-second-order model is closer to the experimental values. These results indicate that the main adsorption mode between uranyl ions and MBF-g-P(AO-*co*-AA) is chemisorption.

To investigate the effect of initial uranium concentration on the equilibrium adsorption capacity of the MBF-g-P(AO-*co*-AA), uranium adsorption tests are performed at initial concentrations (C_0) of uranium from 0 to 45 ppm. As shown in Fig. 6c, with the increase in C_0, the quantity of uranium adsorbed on MBF-g-P(AO-*co*-AA) gradually rises and eventually reaches a plateau, indicating that the adsorption capacity of MBF-g-P(AO-*co*-AA) reaches its maximum (~400 mg g^{-1}). To further understand the

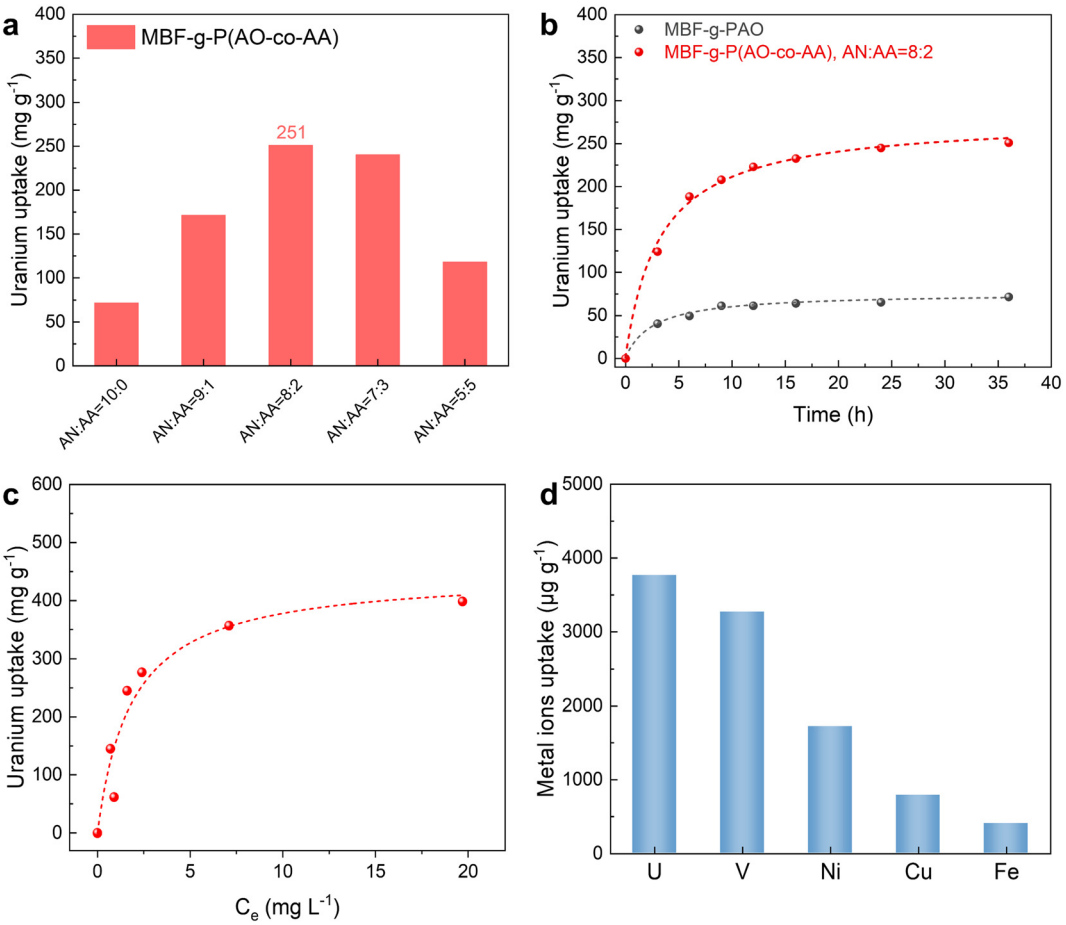

Fig. 6 (a) Uranium adsorption capacity of the MBF-g-P(AO-*co*-AA) prepared with different monomer ratios; adsorption kinetics (b) and adsorption isotherms (c) of the MBF-g-P(AO-*co*-AA); (d) adsorption selectivity in simulated seawater.

Table 1 Kinetic fitting results for uranium adsorption on MBF-g-P(AO-*co*-AA) and MBF-g-PAO

	$Q_{e,exp.}$	Pseudo-first-order model			Pseudo-second-order model		
	(mg g^{-1})	Q_e (mg g^{-1})	k_1 (h^{-1})	R^2	Q_e (mg g^{-1})	k_2 (g mg^{-1} h^{-1})	R^2
MBF-g-P(AO-*co*-AA)	251	190	0.1488	0.9796	270	0.3425	0.9992
MBF-g-PAO	72	42	0.0973	0.8212	76	0.3475	0.9973

Table 2 Isotherm fitting results for uranium adsorption on MBF-g-P(AO-*co*-AA)

	Langmuir parameters			Freundlich parameters		
	Q_m (mg g^{-1})	k_L (L mg^{-1})	R^2	n	k_F (mg g^{-1} (L mg^{-1})$^{1/n}$)	R^2
MBF-g-P(AO-*co*-AA)	455	0.4074	0.9512	2.330	138	0.6214

isothermal adsorption process of the adsorbent material, the experimental results are fitted using the Langmuir and the Freundlich models. Table 2 shows that the uranium adsorption process of MBF-g-P(AN-*co*-AA) is more consistent with the Langmuir model (R^2 = 0.9512) compared to the Freundlich model (R^2 = 0.6214), with a fitted maximum uranium adsorption capacity of 455 mg g^{-1}. In other words, the adsorption of uranyl ions on the MBF-g-P(AN-*co*-AA) is monolayer adsorption and the adsorption sites are uniformly distributed.[24]

Adsorption selectivity is another vital performance indicator for seawater uranium extraction adsorbents due to the low concentration of uranium and the presence of abundant coexisting metal ions in seawater. As shown in Fig. 6d, the adsorption selectivity of MBF-g-P(AN-*co*-AA) in simulated seawater containing multicomponent coexisting metal ions has been investigated. The MBF-g-P(AN-co-AA) exhibits the highest adsorption of uranium, surpassing Ni, Cu, and Fe by 2 to 9 times, with vanadium being the only exception. The competitive adsorption of uranium and vanadium is a common challenge for amidoxime adsorbents, which is affected by the ratio of open-chain (preferentially adsorbing uranium) to cyclic amidoxime groups (preferentially adsorbing vanadium) in the adsorbent.[20,41–43] In our study, the uranium adsorption capacity (3.8 mg g^{-1}) is slightly higher than vanadium adsorption (3.2 mg g^{-1}), suggesting the presence of both forms of amidoxime groups in the MBF-g-P(AO-co-AA), with a slightly higher proportion of the open-chain form. Compared to other amidoxime adsorbents reported in the literature (Table S1†), our adsorbent has a higher uranium adsorption capacity in spiked uranium solutions, particularly in comparison to those prepared by the grafting method. However, due to the competitive adsorption of vanadium, the uranium adsorption capacity in simulated seawater is relatively lower. Through strategies such as adjusting the co-monomers and optimizing the alkaline treatment process,[22,44] it may be possible to further enhance the uranium adsorption selectivity and capacity of the material.

After uranium is adsorbed on the adsorbent, the regeneration ability of the MBF-g-P(AO-*co*-AA) is evaluated by immersing the adsorbent in the elution solution (0.5 M HCl) and monitoring the uranium concentration in the eluent. As shown in Fig. 7a, the yellow color of the uranium-loaded fabric rapidly faded after immersion in 0.5 M HCL. The uranium elution percentage reaches 88% in only 2 min and 93% of uranium is eluted from the adsorbent within 25 min. In contrast, the uranium elution rate is less than 4% after 25 min when the adsorbent is immersed in deionized water. To evaluate the reusability of the adsorbent, five continuous adsorption–desorption cycles are carried out. As shown in Fig. 7b, the uranium adsorption capacity of the adsorbent gradually decreases with the number of cycles. After 5 cycles, the uranium adsorption capacity decreases by 50%. Considering the degradation of the amidoxime group under

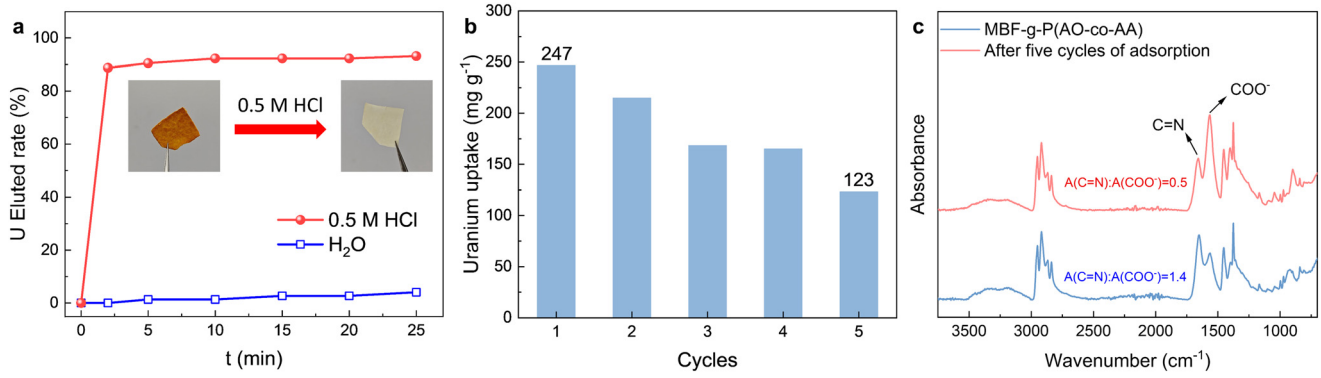

Fig. 7 (a) Elution efficiency of uranium in 0.5 M HCl and H_2O; (b) uranium adsorption performance during 5 adsorption–desorption cycles; (c) the FTIR spectra of MBF-g-P(AO-*co*-AA) initially and after five cycles of adsorption.

acidic and alkaline conditions, the decrease of adsorption performance in recycling is reasonable.[44,45] After five cycles of adsorption, the intensity of C=N relative to that of $-COO^-$ in the IR spectra (Fig. 7c) decreases significantly, suggesting the conversion of the amidoxime group to a carboxyl group.

Alternative to conventional approaches using elution solutions to extract the uranium, we propose direct incineration of the adsorbent for uranium recovery, aiming to minimize the use of chemical reagents. Fig. 8a shows that the fabric with adsorbed uranium turns into a yellow powder after being burned in oxygen. EDS spectroscopic analysis (Fig. 8b and c) shows that prior to incineration, the fabric consists of carbon (mass fraction 57%), oxygen (20%), and uranium (12%). After incineration, the carbon is converted to CO_2 gas and leaves, and most of the remaining is uranium (49%) and oxygen (26%). The sodium in the materials comes from the conversion of the –COOH into –COONa during the amidoxime reaction. Due to our lower cost of adsorbent production, direct incineration of inexpensive sorbents to recover high-value uranium may be a potentially more convenient and feasible option.

3 Conclusions

In summary, we have evaluated the bulk photografting technology to economically and rapidly produce amidoxime-functionalized melt-blown nonwoven fabric. The cyano group can be introduced to the surface of the fabric within 3 min by photografting with a DOG of more than 100%, and the reagent consumption is less than 1/5 of that used for traditional surface graft polymerization in solution. These advantages are important for feasible continuous production of the material, potentially lowering the cost of the uranium adsorbent.

The fiber morphology and mechanical properties of the nonwoven fabrics are retained after surface functionalization. The uranium adsorption test proves that the fabrics have good uranium adsorption capacity and selectivity of the amidoxime adsorbents. The optimal equilibrium of the adsorption sites and hydrophilic group composition is reached when the feeding monomer ratio is AN : AA = 8 : 2, resulting in the highest uranium adsorption performance of the material (with a fitted maximum uranium adsorption of 455 mg g^{-1}). Moreover, as an alternative method to recover uranium, a powder containing 49% uranium mass fraction is obtained by directly incinerating the uranium adsorbed fabric. This rapid, efficient and economic bulk photografting technology may be promising for the industrialized production of amidoxime adsorbents for extraction of uranium from seawater.

4 Experimental section

4.1 Materials

The melt-blown nonwoven fabric (MBF) (25 g m^{-2}, BFE99) was purchased from Mingyu Nonwoven Fabric Co., Ltd (Hunan). Acrylonitrile (AN), acrylic acid (AA), ethanol (EtOH), and dimethylformamide (DMF) were of analytical grade and obtained from Sinopharm Chemical Reagent Company (Beijing). Benzophenone (BP, 99%), hydroxylamine hydrochloride ($NH_2OH{\cdot}HCl$, 98.5%) and 1000 ppm vanadium (V), nickel (Ni), copper (Cu), and iron (Fe) standard solutions were purchased from J&K Scientific Ltd (Beijing). 1000 ppm uranium standard solution was purchased from Macklin Inc (Shanghai). Sea salt was purchased from Zancheng Technology Co. (Tianjin). Fluorinated ethylene propylene (FEP) films was purchased from Zhanyang Polymer Material Co., Ltd (Dongguan). Acrylonitrile and acrylic acid were purified by distillation under reduced pressure before use, and other reagents were used without any further purification.

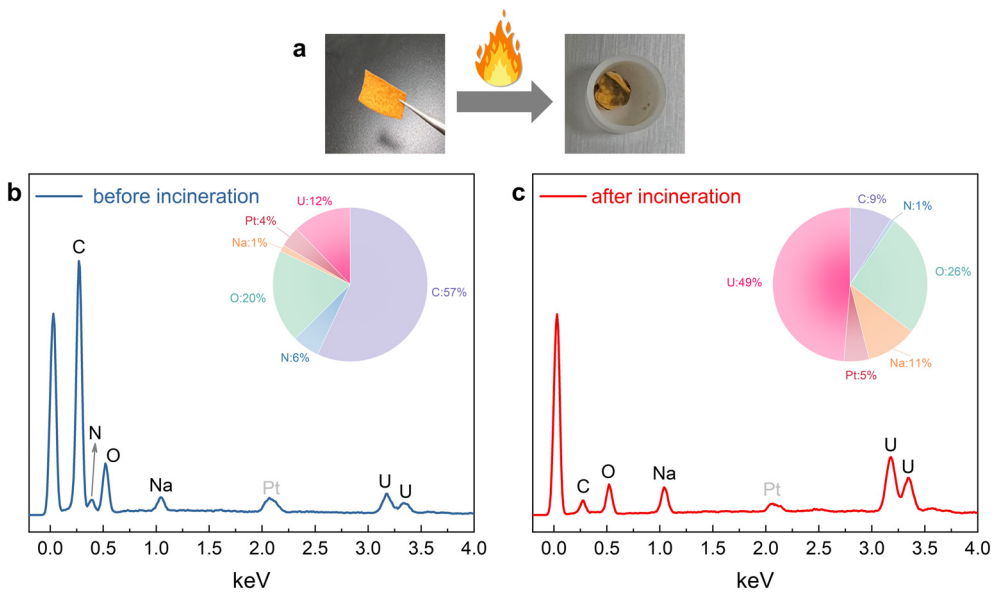

Fig. 8 (a) Photos and (b and c) SEM EDS spectra of fabric before and after incineration.

4.2 Surface photografting polymerization of AN and AA

In the first step, AN and AA were photograft-polymerized onto the commercial MBF to obtain MBF-g-P(AN-*co*-AA). BP ranging from 0 to 270 mg mL^{-1} was added to the AN/AA mixture (v/v ratios of 10 : 0, 9 : 1, 8 : 2, 7 : 3, and 5 : 5, corresponding to molar ratios of 10 : 0, 9.4 : 1, 8.4 : 2, 7.3 : 3, and 5.2 : 5, respectively) to prepare the photografting solution. Subsequently, 150 μL of the above solution was applied to a 30 mg MBF positioned on a FEP film. Then an additional FEP film was placed on top to ensure uniform solution spreading. The films were assembled between two quartz plates to secure the setup and then exposed to irradiation for 0 to 5 min using a 300 W high-pressure mercury lamp (light intensity 72 mW cm^{-2} at λ = 365 nm). The FEP films were placed in between the MBF and the quartz plates only to prevent contamination of the latter by the reaction mixture. Afterwards, the MBF-g-P(AN-*co*-AA) underwent thorough rinsing with DMF and ethanol, dried overnight at 45 °C under vacuum, and stored in a sealed container before the subsequent treatment. The degree of grafting (DOG) was calculated using eqn (1):

$$\mathrm{DOG} = (w_1 - w_0)/w_0 \quad (1)$$

where w_0 (mg) and w_1 (mg) are the weight of MBF and MBF-g-P(AN-*co*-AA), respectively.

4.3 Amidoximation of MBF-g-P(AN-*co*-AA)

The amidoximation of the cyano groups is carried out by the reaction with hydroxylamine. The specific steps are as follows: 5.0 g $NH_2OH{\cdot}HCl$ was dissolved in 100 mL of demineralized water, then the solution was neutralized by the addition of NaOH (2.9 g). Subsequently, the MBF-g-P(AN-*co*-AA) was immersed in the solution and stirred at 60 °C for 1 to 3 h. After that, the sample (designated as MBF-g-P(AO-*co*-AA)) underwent thorough rinsing with water and ethanol and was subsequently dried overnight at 40 °C in a vacuum oven. The amidoxime densities (AO density, mmol g^{-1}) was estimated using eqn (2):

$$\text{AO density} = 1000(w_2 - w_1)/33w_2 \quad (2)$$

where w_1 (mg) and w_2 (mg) are the weight of MBF-g-P(AN-*co*-AA) and MBF-g-P(AO-*co*-AA), respectively.

4.4 Characterization

The Fourier-transform infrared (FTIR) spectra of the material were analyzed using a Thermo Fisher Nicolet iS50 spectrometer (USA) equipped with a diamond attenuated total reflectance accessory. X-ray photoelectron spectroscopy (XPS) measurements were conducted on a Thermo Fisher ESCALB Xi+ instrument (USA). Scanning electron microscope (SEM) images and energy-dispersive X-ray spectroscopy (EDS) spectra were acquired using a Zeiss Merlin microscope (Germany). The concentrations of uranium and other metal ions were determined through inductively coupled plasma optical emission spectrometry (ICP-OES, Spectro Arcos FHX22, Germany) and inductively coupled plasma mass spectrometry (ICP-MS, Agilent 7800, USA). Thermal degradation of polymers was tested using a thermogravimetric analysis (TGA) Instrument (Mettler TGA/DSC1/1600HT, Switzerland) in an oxygen atmosphere. The specific surface areas of the fabrics were determined from the nitrogen adsorption–desorption isotherms obtained at 77 K using an Autosorb NOVA 2200e analyzer (Quantachrome, USA). The specific surface areas were calculated by the Brunauer–Emmett–Teller (BET) method. The mechanical properties were investigated using a universal testing machine (68TM-30, Instron, USA). The tensile test samples are rectangular specimens with a test area of 20 mm × 20 mm × 0.038 mm (length × width × thickness). The running speed of the tensile test is 20 mm min^{-1}.

4.5 Uranium adsorption experiments

The uranium adsorption experiments of MBF-g-P(AO-*co*-AA) were conducted in uranium-spiked water. Following the protocols in the literature, all adsorbents underwent a 0.5-hour treatment in a 2.5 wt% KOH aqueous solution at 60 °C to facilitate the deprotonation of amidoxime (AO) groups, enhancing their binding capacity toward uranyl ions.[44,46] Uranium-spiked aqueous solutions with varying concentrations were prepared by diluting the 1000 ppm uranium standard solution with an appropriate amount of distilled water. The solution's pH was adjusted to 6.0 ± 0.1 using either HCl or NaOH aqueous solution. The thoroughly washed 12 mg of MBF-g-P(AO-*co*-AA) was added into a 200 mL uranium-spiked aqueous solution on a rotary shaker (120 rpm) at 25 °C for the adsorption experiments. All adsorption tests were conducted with a contact time of 36 h. The uranium concentrations in the solution were measured using ICP-OES. The adsorption capacity (Q_t) was calculated using eqn (3):

$$Q_t = (C_0 - C_t)V/m \quad (3)$$

where Q_t (mg g^{-1}) is the adsorption capacity of MBF-g-P(AO-*co*-AA) at time t, C_0 and C_t (mg L^{-1}) are the initial and instantaneous concentrations of uranium, respectively, V (L) is the volume of the solution, and m (g) is the mass of MBF-g-P(AO-*co*-AA).

4.6 Selective adsorption

A selective adsorption experiment was performed using simulated seawater. In line with prior literature,[23,34] a simulated seawater solution was prepared with concentrations of U, V, Fe, Ni, and Cu set at 100 times that of natural seawater by adding standard solutions of metal ions into the sea salt aqueous solution (providing sodium (Na), potassium (K), and magnesium (Mg) ions), with the concentration of Na ion being 1.3 × 10^4 mg L^{-1}, which is close to the concentration of Na ion in seawater.

Subsequently, 12 mg of MBF-g-P(AO-*co*-AA) was added into 200 mL of the aforementioned simulated seawater and shaken on a shaking bath for 36 h. The initial and final concentrations of metal ions were determined using ICP-MS.

4.7 Desorption and reusability

Adsorption–desorption experiments were performed for 5 continuous cycles to evaluate the reusability of the MBF-g-P(AO-*co*-AA). The adsorption experiments were carried out in 20 ppm uranium-spiked solution as mentioned above. After the adsorption experiment, the U-adsorbed fabric was immersed in 0.5 M HCl and stirred at room temperature for 25 min to accomplish the desorption experiment. The uranium elution rate was calculated using eqn (4):

$$\text{elution rate} = C_t V/m \quad (4)$$

where C_t (mg L^{-1}) is the instantaneous concentration of uranium, V (L) is the volume of the eluent, and m (mg) is the mass of adsorbed uranium. After the elution was completed, the fabric was washed with deionized water three times and then prepared for the next adsorption experiment.

Data availability

The data supporting this article are available within the article and its ESI.† If necessary, the raw data are available on request to the corresponding author.

Conflicts of interest

The authors declare no conflict of interest.

Acknowledgements

This work was supported by internal funds from Tsinghua University.

References

1 B. W. Brook, A. Alonso, D. A. Meneley, J. Misak, T. Blees and J. B. van Erp, Why nuclear energy is sustainable and has to be part of the energy mix, *Sustainable Mater. Technol.*, 2014, **1–2**, 8–16.
2 Nuclear Energy Agency and International Atomic Energy Agency, *Uranium 2022: Resources, production and demand*, OECD Publishing Paris, 2023.
3 Y. Xie, Z. Y. Liu, Y. Geng, H. Li, N. Wang, Y. Song, X. Wang, J. Chen, J. Wang, S. Ma and G. Ye, Uranium extraction from seawater: Material design, emerging technologies and marine engineering, *Chem. Soc. Rev.*, 2023, **52**, 97–162.
4 Z. Y. Liu, Y. Xie, Y. Wang, T. Hu, G. Ye and J. Chen, Recent advances in sorbent materials for uranium extraction from seawater, *Qinghua Daxue Xuebao*, 2021, **61**, 279–301.
5 C. W. Abney, R. T. Mayes, T. Saito and S. Dai, Materials for the recovery of uranium from seawater, *Chem. Rev.*, 2017, **117**, 13935–14013.
6 I. Ioannidis, I. Pashalidis, B. Mulla, G. Kotanidis, K. Ioannou, G. Constantinides, N. Kostoglou and C. Rebholz, Radionuclide removal from aqueous solutions using oxidized carbon fabrics, *Materials*, 2023, **16**, 7479.
7 M. Tuzen, T. A. Saleh, A. Sarı and N. Ullah, Interfacial polymerization of trimesoyl chloride with melamine and palygorskite for efficient uranium ions ultra-removal, *Chem. Eng. Res. Des.*, 2020, **159**, 353–361.
8 E. Bağda, M. Tuzen and A. Sarı, Equilibrium, thermodynamic and kinetic investigations for biosorption of uranium with green algae (Cladophora hutchinsiae), *J. Environ. Radioact.*, 2017, **175–176**, 7–14.
9 T. A. Saleh, M. Tuzen Naeemullah and A. Sarı, Polyethylenimine modified activated carbon as novel magnetic adsorbent for the removal of uranium from aqueous solution, *Chem. Eng. Res. Des.*, 2017, **117**, 218–227.
10 T. Xiong, Q. Li, J. Liao, Y. Zhang and W. Zhu, Highly enhanced adsorption performance to uranium(VI) by facile synthesized hydroxyapatite aerogel, *J. Hazard. Mater.*, 2022, **423**, 127184.
11 E. Georgiou, G. Raptopoulos, M. Papastergiou, P. Paraskevopoulou and I. Pashalidis, Extremely efficient uranium removal from aqueous environments with polyurea-cross-linked alginate aerogel beads, *ACS Appl. Polym. Mater.*, 2022, **4**, 920–928.
12 M. Zhao, A. Tesfay Reda and D. Zhang, Reduced graphene oxide/ZIF-67 aerogel composite material for uranium adsorption in aqueous solutions, *ACS Omega*, 2020, **5**, 8012–8022.
13 T. Liu, Z. Li, X. Zhang, H. Tan, Z. Chen, J. Wu, J. Chen and H. Qiu, Metal-organic framework-intercalated graphene oxide membranes for selective separation of uranium, *Anal. Chem.*, 2021, **93**, 16175–16183.
14 J. E. Quinn, D. S. Sedger, A. T. Brennan, R. J. Ring and K. Soldenhoff, Recovery of uranium from carbonate solutions using Lewatit TP 107 resin, *Hydrometallurgy*, 2020, **194**, 105360.
15 C. Wang, A. S. Helal, Z. Wang, J. Zhou, X. Yao, Z. Shi, Y. Ren, J. Lee, J. K. Chang, B. Fugetsu and J. Li, Uranium in situ electrolytic deposition with a reusable functional graphene-foam electrode, *Adv. Mater.*, 2021, **33**, 2102633.
16 D. Chen, Y. Li, X. Zhao, M. Shi, X. Shi, R. Zhao and G. Zhu, Self-standing porous aromatic framework electrodes for efficient electrochemical uranium extraction, *ACS Cent. Sci.*, 2023, **9**, 2326–2332.
17 R. V. Davies, J. Kennedy, K. M. Hill, R. W. Mcilroy and R. Spence, Extraction of uranium from sea water, *Nature*, 1964, **203**, 1110–1115.
18 H. Egawa and H. Harada, Recovery of uranium from seawater by using chelating resins containing amidoxime groups, *Nippon Kagaku Kaishi*, 1979, **7**, 958–959.
19 S. Vukovic, B. P. Hay and V. S. Bryantsev, Predicting stability constants for uranyl complexes using density functional theory, *Inorg. Chem.*, 2015, **54**, 3995–4001.
20 A. S. Ivanov, C. J. Leggett, B. F. Parker, Z. C. Zhang, J. Arnold, S. Dai, C. W. Abney, V. S. Bryantsev and L. F. Rao,

Origin of the unusually strong and selective binding of vanadium by polyamidoximes in seawater, *Nat. Commun.*, 2017, **8**, 1560.

21 N. Tang, J. Liang, C. G. Niu, H. Wang, Y. Luo, W. L. Xing, S. J. Ye, C. Liang, H. Guo, J. Y. Guo, Y. F. Zhang and G. M. Zeng, Amidoxime-based materials for uranium recovery and removal, *J. Mater. Chem. A*, 2020, **8**, 7588–7625.

22 X. L. He, H. C. Deng, H. Wu, W. Yu, Z. M. Guo and X. M. Liang, Amidoxime-based polymer microspheres with high selectivity for uranium from saline lake brine, *ACS Appl. Polym. Mater.*, 2023, **5**, 4380–4387.

23 D. Wang, J. A. Song, J. Wen, Y. H. Yuan, Z. L. Liu, S. Lin, H. Y. Wang, H. L. Wang, S. L. Zhao, X. M. Zhao, M. H. Fang, M. Lei, B. Li, N. Wang, X. L. Wang and H. Wu, Significantly enhanced uranium extraction from seawater with mass produced fully amidoximated nanofiber adsorbent, *Adv. Energy Mater.*, 2018, **8**, 1802607.

24 Z. Y. Liu, Y. S. Lan, J. F. Jia, Y. Y. Geng, X. B. Dai, L. T. Yan, T. Y. Hu, J. Chen, K. Matyjaszewski and G. Ye, Multi-scale computer-aided design and photo-controlled macromolecular synthesis boosting uranium harvesting from seawater, *Nat. Commun.*, 2022, **13**, 3918.

25 D. Chen, X. Zhao, M. Shi, X. Fu, W. Hu, X. Shi, R. Zhao and G. Zhu, Enhanced and selective uranium extraction onto electrospun nanofibers by regulating the functional groups and photothermal conversion performance, *Chem. Eng. J.*, 2024, **480**, 148108.

26 D. Chen, X. Zhao, X. Jing, R. Zhao, G. Zhu and C. Wang, Bio-inspired functionalization of electrospun nanofibers with anti-biofouling property for efficient uranium extraction from seawater, *Chem. Eng. J.*, 2023, **465**, 142844.

27 S. Shi, Y. X. Qian, P. P. Mei, Y. H. Yuan, N. Jia, M. Y. Dong, J. C. Fan, Z. H. Guo and N. Wang, Robust flexible poly(amidoxime) porous network membranes for highly efficient uranium extraction from seawater, *Nano Energy*, 2020, **71**, 104629.

28 C. X. Ma, J. X. Gao, D. Wang, Y. H. Yuan, J. Wen, B. J. Yan, S. L. Zhao, X. M. Zhao, Y. Sun, X. L. Wang and N. Wang, Sunlight polymerization of poly(amidoxime) hydrogel membrane for enhanced uranium extraction from seawater, *Adv. Sci.*, 2019, **6**, 1900085.

29 S. H. Choi and Y. C. Nho, Radiation-induced graft copolymerization of binary monomer mixture containing acrylonitrile onto polyethylene films, *Radiat. Phys. Chem.*, 2000, **58**, 157–168.

30 S. H. Choi and Y. C. Nho, Adsorption of UO_2^{2+} by polyethylene adsorbents with amidoxime, carboxyl, and amidoxime/carboxyl group, *Radiat. Phys. Chem.*, 2000, **57**, 187–193.

31 T. Saito, S. Brown, S. Chatterjee, J. Kim, C. Tsouris, R. T. Mayes, L. J. Kuo, G. Gill, Y. Oyola, C. J. Janke and S. Dai, Uranium recovery from seawater: Development of fiber adsorbents prepared via atom-transfer radical polymerization, *J. Mater. Chem. A*, 2014, **2**, 14674–14681.

32 Z. Xing, J. T. Hu, M. H. Wang, W. L. Zhang, S. N. Li, Q. H. Gao and G. Z. Wu, Properties and evaluation of amidoxime-based UHMWPE fibrous adsorbent for extraction of uranium from seawater, *Sci. China: Chem.*, 2013, **56**, 1504–1509.

33 T. L. Prasad, P. K. Tewari and D. Sathiyamoorthy, Parametric studies on radiation grafting of polymeric sorbents for recovery of heavy metals from seawater, *Ind. Eng. Chem. Res.*, 2010, **49**, 6559–6565.

34 R. Yu, X. S. Zhang, Y. R. Lu, W. Chen, X. Chen and L. B. Li, Advanced amidoximated polyethylene nanofibrous membranes for practical uranium extraction from seawater, *ACS Sustainable Chem. Eng.*, 2022, **10**, 12307–12318.

35 C. K. Na, H. J. Park and B. G. Kim, Optimal amidoximation conditions of acrylonitrile grafted onto polypropylene by photoirradiation-induced graft polymerization, *J. Appl. Polym. Sci.*, 2012, **125**, 776–785.

36 W. T. Yang and B. Rånby, Bulk surface photografting process and its applications. I. Reactions and kinetics, *J. Appl. Polym. Sci.*, 1996, **62**, 533–543.

37 J. P. Deng, L. F. Wang, L. Y. Liu and W. T. Yang, Developments and new applications of UV-induced surface graft polymerizations, *Prog. Polym. Sci.*, 2009, **34**, 156–193.

38 Y. Oyola and S. Dai, High surface-area amidoxime-based polymer fibers co-grafted with various acid monomers yielding increased adsorption capacity for the extraction of uranium from seawater, *Dalton Trans.*, 2016, **45**, 8824–8834.

39 W. T. Yang and B. Rånby, Bulk surface photografting process and its applications. II. Principal factors affecting surface photografting, *J. Appl. Polym. Sci.*, 1996, **62**, 545–555.

40 X. Xu, L. Xu, J. Ao, Y. Liang, C. Li, Y. Wang, C. Huang, F. Ye, Q. Li, X. Guo, J. Li, H. Wang, S. Ma and H. Ma, Ultrahigh and economical uranium extraction from seawater via interconnected open-pore architecture poly(amidoxime) fiber, *J. Mater. Chem. A*, 2020, **8**, 22032–22044.

41 X. Zhang, D. G. Li, C. Cui, S. S. Chen, M. Ji, W. W. Tang, L. Yang, F. Q. Zhang, J. Y. Li, D. X. Zhang and X. Y. Xu, Alginate-based supermacroporous hydrogels fabricated by cryo-polymerization for uranium extraction from seawater, *Polym. Chem.*, 2023, **14**, 2902–2915.

42 D. Wang, J. Song, S. Lin, J. Wen, C. Ma, Y. Yuan, M. Lei, X. Wang, N. Wang and H. Wu, A marine inspired hybrid sponge for highly efficient uranium extraction from seawater, *Adv. Funct. Mater.*, 2019, **29**, 1901009.

43 X. Xu, H. Zhang, J. Ao, L. Xu, X. Liu, X. Guo, J. Li, L. Zhang, Q. Li, X. Zhao, B. Ye, D. Wang, F. Shen and H. Ma, 3D hierarchical porous amidoxime fibers speed up uranium extraction from seawater, *Energy Environ. Sci.*, 2019, **12**, 1979–1988.

44 H. B. Pan, L. J. Kuo, J. Wood, J. Strivens, G. A. Gill, C. J. Janke and C. M. Wai, Towards understanding KOH conditioning of amidoxime-based polymer adsorbents for sequestering uranium from seawater, *RSC Adv.*, 2015, **5**, 100715–100721.

45 S. O. Kang, S. Vukovic, R. Custelcean and B. P. Hay, Cyclic imide dioximes: Formation and hydrolytic stability, *Ind. Eng. Chem. Res.*, 2012, **51**, 6619–6624.

46 D. S. Bolotin, N. A. Bokach and V. Y. Kukushkin, Coordination chemistry and metal-involving reactions of amidoximes: Relevance to the chemistry of oximes and oxime ligands, *Coord. Chem. Rev.*, 2016, **313**, 62–93.